



# A comparative study on the Cs adsorption/desorption and structural changes in different clay minerals

In-Ho Yoon<sup>1</sup> · Sang-Ho Lee<sup>2</sup> · Ilgook Kim<sup>1</sup> · Sung Man Kim<sup>1</sup>

Received: 24 November 2023 / Accepted: 4 March 2024 / Published online: 12 March 2024  
© The Author(s), under exclusive licence to Springer-Verlag GmbH Germany, part of Springer Nature 2024

## Abstract

We investigated the structural changes in clay minerals after Cs adsorption and understood their low desorption efficiency using an ion-exchanger. We focused on the role of interlayers in Cs adsorption and desorption in 2:1 clay minerals, namely illite, hydrobiotite, and montmorillonite, using batch experiments and XRD and EXAFS analyses. The adsorption characteristics of the clay minerals were analyzed using cation exchange capacity (CEC), maximum adsorption isotherms ( $Q_{\max}$ ), and radiocesium interception potential (RIP) experiments. Although illite showed a low CEC value, it exhibited high selectivity for Cs with a relatively high RIP/CEC ratio. The Cs desorption efficiency after treatment with a NaCl ion exchanger was the highest for illite (74.3%), followed by hydrobiotite (45.5%) and montmorillonite (30.3%); thus, Cs adsorbed onto planar sites, rather than on interlayers or frayed edge sites (FESs), is easily desorbed. After NaCl treatment, XRD analysis showed that the low desorption efficiency was due to the collapse of the interlayer-fixed Cs, which tightly narrowed the interlayers' hydrobiotite due to the ion exchange of divalent cations ( $Mg^{2+}$  or  $Ca^{2+}$ ) into the monovalent cation ( $Na^+$ ). Moreover, EXAFS analysis showed that hydrobiotite formed inner-sphere structures after NaCl desorption, indicating that it was difficult to remove Cs from NaCl desorption due to the collapsed hydrobiotite and montmorillonite interlayers as well as the strong bonding in FESs of illite. In contrast, chelation desorption using oxalic acid effectively dissolved the narrowed interlayers of hydrobiotite (98%) and montmorillonite (85.26%), enhancing the desorption efficiency. Therefore, low desorption efficiency for Cs clays using an ion exchanger was caused by the collapsed interlayer due to the exchange between monovalent cation and divalent cation.

**Keywords** Cesium · Clay · Interlayer · Adsorption · Desorption · Extended X-ray absorption fine structure

## Introduction

Accidental radioactive cesium (Cs) release from nuclear facilities results in soil waste contamination (Ding et al. 2016; Yamamoto 2012). The 2:1 clay minerals commonly found in soil bind strongly to radioactive Cs, impeding soil remediation (Cornell 1993; Nagy et al. 1999). These

minerals exhibit different adsorption and desorption behaviors owing to their unique properties. For instance, Cs adsorption on kaolinite occurs mainly on the outer surfaces of the particles and is easily exchanged (Kim et al. 1996b; Miranda-Trevino & Coles 2003).

Common 2:1 phyllosilicates, such as montmorillonite, hydrobiotite, and illite, have identical fundamental structures but different expansivity owing to varying net negative charge densities resulting from isomorphic substitutions. They also have additional Cs adsorption sites, such as frayed edge sites (FESs), that adsorb Cs in a stable state, as well as hydration or dehydration interlayer sites (Bradbury & Baeyens 2000; Mukai et al. 2014; Okumura et al. 2013; Poinssot et al. 1999). Weathering-induced interlayer contraction stabilizes combined Cs (Kim et al. 2017; Kogure et al. 2012; Tamura et al. 2014). Radionuclide adsorption in montmorillonite and vermiculite occurs mainly via ion exchange and surface complexation, whereas surface complexation

---

Responsible Editor: Tito Roberto Cadaval Jr

✉ In-Ho Yoon  
ihyoona@kaeri.re.kr

<sup>1</sup> Decommissioning Technology Research Division, Korea Atomic Energy Research Institute, 989-111, Daedeok-Daero, Yuseong-Gu, Daejeon 34057, Republic of Korea

<sup>2</sup> Disposal Performance Demonstration Research Division, Korea Atomic Energy Research Institute, Daedeok-Daero 989-111, Yuseong-Gu, Daejeon 305-353, Republic of Korea

seldom co-occurs with ion exchange in illite (Tournassat et al. 2018; Zhang et al. 2017). In acidic environments, ion exchange at permanently charged basal or interlayer sites predominates radionuclide adsorption onto clay minerals. In contrast, surface complexation predominates at high pH in variable charge-edge locations, which highly depend on pH (Abollino et al. 2008; Bourg et al. 2007; Tan et al. 2010; Wu et al. 2018; Zhang et al. 2011).

In swellable phyllosilicates such as montmorillonite and hydrobiotite, interlayer spacing affects the cation exchange capacity (CEC), which is principally associated with ion exchange (Chen & Dong 2013). X-ray diffraction (XRD) has shown that phlogopite becomes montmorillonite-like during Th(IV) adsorption, indicating that the clay mineral interlayer is crucial for radionuclide adsorption because it affects the CEC and interlayer distance (Han et al. 2023). Ion exchange reversibly adsorbs Cs onto montmorillonite at low concentrations; however, at high concentrations, it becomes fixed, and the basal spacing decreases with increasing Cs concentration (Iijima et al. 2010). Therefore, Cs can be fixed in FESs of illite and the interlayers of other 2:1 expansive clay minerals. More FESs can be produced in micaceous minerals, and more irreversibly fixed Cs can accumulate because of weathering and acidification. However, the clay mineral characteristics may be altered by the irreversible fixing of Cs in interlayers (Hwang et al. 2023; Park et al. 2019b; Wang et al. 2023; Zhang et al. 2022).

Extended X-ray absorption fine structure (EXAFS) studies have demonstrated that Cs can be adsorbed onto the regular exchangeable sites, FESs, and interlayer sites of phyllosilicate minerals in soil (Bostick et al. 2002;

Fan et al. 2014a, 2014b; Park et al. 2019a). On planar or interlayer sites, hydrated Cs<sup>+</sup> ions can form outer-sphere (OS) complexes, whereas dehydrated Cs<sup>+</sup> ions can form inner-sphere (IS) complexes at FESs or interlayer sites. OS complexes are extractable using alkaline ions, whereas IS complexes are not extractable (Fan et al. 2014b; Qin et al. 2012; Zhang et al. 2023). Their effects on desorption efficiency and structural changes were analyzed using XRD and EXAFS for each clay mineral. The objectives of this study were to investigate the adsorption characteristics (CEC, radiocesium interception potential (RIP), and Cs adsorption capacity), desorption characteristics (NaCl and oxalic acid), and understand their low desorption efficiency using ion-exchanger (Fig. 1).

## Materials and methods

### Materials

Illite (2500 mesh, < 5 μm, Youngkoong Illite Co., Ltd.) and montmorillonite (20 μm) (SAz-1, Clay Minerals Society, USA) were used as received. Hydrobiotite (Sigma-Aldrich) used in this study was ground in a milling machine and sieved to achieve a particle size below 20 μm and air-dried at room temperature. Chloride salts (NH<sub>4</sub>Cl, MgCl<sub>2</sub>, and CaCl<sub>2</sub>) as well as the CsCl used in the adsorption experiments were purchased from Sigma-Aldrich. Oxalic acid dihydrate and NaCl were used as desorbents (Sigma-Aldrich) to extract Cs from the clay minerals.

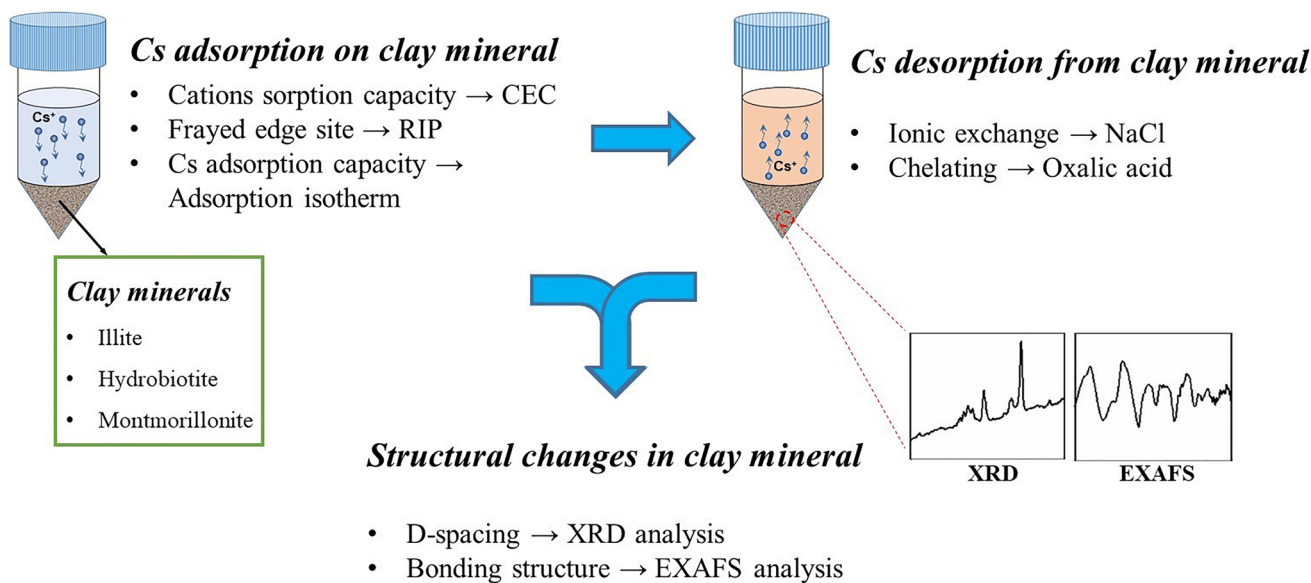


Fig. 1 Schematic diagram of Cs adsorption/desorption and structural changes in different clay minerals

### Cation exchange capacity (CEC) analysis

According to the previous study (Kim et al. 2020a; Park et al. 2021b), montmorillonite, hydrobiotite, and illite (6 g) were combined with a 1 N sodium acetate solution (pH 8.2, 33 mL) in a shaking incubator for 10 min and then centrifuged to separate the components. Three fresh sodium acetate solutions were obtained using this method. The clays were mixed with isopropanol (> 99%, 33 mL) for 10 min in the shaking incubator before centrifugation to separate the components. This was performed twice. The clays were mixed with an ammonium acetate solution (1 N, pH 7, 33 mL), and the supernatant was recovered after centrifugation. The supernatant was then filtered using a polyvinylidene difluoride (PVDF) membrane filter (0.2- $\mu\text{m}$  pore size) after this process was repeated twice. Atomic Absorption Spectroscopy (Analytik Jena ContraAA 700) was used to quantify  $\text{Na}^+$  ions in the supernatant, and the amount of  $\text{Na}^+$  desorbed per unit mass of clay was used to compute the CECs of montmorillonite, hydrobiotite, and illite.

### Radiocesium interception potential (RIP) analysis

Montmorillonite, hydrobiotite, and illite (0.1 g) were dispersed in an aqueous solution (5 mL) of 0.1 M  $\text{CaCl}_2$  and 0.5 mM KCl and sealed in a dialysis membrane (molecular weight cutoff = 6–8 kDa) before incubation in 200 mL of the same medium. According to previous studies (Fan et al. 2014b; Lee et al. 2017; Zachara et al. 2002), the amounts of  $\text{CaCl}_2$  and KCl were adequate to block the planar sites of the clays. A fresh solution was added daily to the medium. After five days, the medium was replaced with a 200-mL aqueous solution containing 0.1 M  $\text{CaCl}_2$ , 0.5 mM KCl, and 0.5 mM CsCl, and the cells were incubated for 24 h. AAS (Analytik Jena contraAA 700) was used to assess unbound Cs and residual K in the medium, and RIP was computed using the following equation:

$$\text{RIP}(\text{mol}/\text{kg}) = K_d^{\text{Cs}} \times [m_K] \quad (1)$$

where  $K_d^{\text{Cs}}$  (L/kg) and  $m_K$  (mol/L) are the distribution coefficient of  $\text{Cs}^+$  ions and the concentration of  $\text{K}^+$  ions in the medium, respectively.

### Cs adsorption kinetics of clay minerals

In batch tests, 0.5 g of each clay was added to a 250-mL polypropylene bottle with a Teflon-sealed top, along with 200 mL of solution of 3.7594-mmol/L Cs concentration. Each clay was stirred in a shaker at  $25 \pm 0.5$  °C and 150 rpm. Sampling was conducted at time points of 0.5, 1, 2.5, 5, 10, 30, 60, 300, and 1440 min, followed by filtration through a

0.2- $\mu\text{m}$  hydrophilic syringe filter to quantify the residual Cs in the solution. The determination of Cs concentration in the solutions was performed using inductively coupled plasma mass spectrometry (ICP-MS, ELAN DRC II, PerkinElmer, USA). The mass balance equation (Eq. 1) was employed to calculate the amount of Cs adsorbed by the adsorbent at each sampling interval:

$$Q_t = ((C_0 - C_t) \times v) / m \quad (1)$$

where  $C_t$  and  $C_0$  are the remaining and initial concentrations (mmol/L), respectively, and  $Q_t$  is the amount of Cs adsorbed at time  $t$  (mmol/g);  $v$  and  $m$  are the volume (L) of solution and mass (g) of adsorbents in each sample.

The intraparticle diffusion model was utilized in this adsorption study to ascertain whether the rate-limiting step corresponds to intraparticle diffusion. The rate parameter for intraparticle diffusion is mathematically expressed as follows (Önal et al. 2006):

$$Q_t = K_{id} t^{1/2} + C \quad (2)$$

where  $K_{id}$  is the intraparticle diffusion rate constant and  $C$  is the intercept.

If the adsorption process adheres to intraparticle diffusion, the plot of  $Q_t$  versus  $t^{1/2}$  would be a straight line and the  $K_{id}$  and  $C$  can be calculated from the slope of the plot.  $C$  gives an idea about the thickness of the boundary layer; i.e., the larger the intercept the greater the boundary layer effect (Önal et al. 2006).

### Cs adsorption isotherms of clay minerals

Clay (0.1 g) and a CsCl solution (50 mL) were combined in deionized water with Cs concentrations ranging from 20 to 800 mg/L ( $1.5 \times 10^{-4}$ – $6.2 \times 10^{-3}$  M). The batch adsorption experiments were performed using a shaking incubator (Vision Scientific, Republic of Korea) under controlled conditions (adsorbent dosage = 2 g/L, agitation speed = 150 rpm, and temperature = 25 °C). Cs sorption was equilibrated by shaking for 24 h at 25 °C. Thereafter, the samples' aqueous phase was filtered using a 0.2- $\mu\text{m}$  syringe filter after centrifugation to separate it from the samples. Residual Cs was detected in the aqueous phase using inductively coupled plasma mass spectrometry (ICP-MS). Using the (3) Freundlich, (4) Dubinin-Radushkevich, (5) Langmuir (6) Sips, and (7) Redlich–Peterson adsorption models to match the Cs sorption isotherms obtained at 25 °C, the sorption properties of Cs were examined.

$$Q_e = K_F C_e^{1/n_e} \quad (3)$$

$$Q_e = Q_{\max} (-\beta \epsilon^2) \quad (4)$$

$$Q_e = Q_{\max} \times KC_e / (1 + KC_e) \quad (5)$$

$$Q_e = (Q_{\max} K_s C_e^{1/n}) / (1 + K_s C_e^{1/n}) \quad (6)$$

$$Q_e = (K_R C_e) / (1 + \alpha R C_e^g) \quad (7)$$

where  $Q_e$  and  $Q_{\max}$  are the adsorbed amount of sorbate (mmol/g clay) and maximum adsorption capacity, respectively;  $C_e$  is the equilibrium concentration of the sorbate in the liquid (mmol/L).  $K_F$  and  $1/n$  are constants indicating the adsorption capacity and intensity, respectively.  $\beta$  ( $\text{mol}^2 \text{kJ}^{-2}$ ) is a constant related to the adsorption energy; and  $\varepsilon$  ( $\text{kJ mol}^{-1}$ ) is the adsorption potential.  $K$  (L/mmol) is a constant representing the affinity between the sorbent and sorbate.  $K_s$  is a constant indicating the affinity for adsorption (L/mg);  $K_R$  is the adsorption capacity constant (L/g); and  $\alpha R$  and  $g$  are the isotherm constant (L/mg) and an exponential factor, respectively.

The fundamental aspect of the Langmuir model can be elucidated through a dimensionless equilibrium parameter ( $R_L$ ), which is defined by the following equation:

$$R_L = 1 / (1 + K_L C_0) \quad (8)$$

where  $C_0$  is the initial Cs concentration (mmol/L) and  $K_L$  is Langmuir isotherm constant.

### Desorption of Cs from clay minerals

In each polypropylene bottle, 35 g of montmorillonite, hydrobiotite, and illite was combined with 350 mL of a 3 mM CsCl aqueous solution, respectively. Each clay was shaken horizontally at room temperature for seven days for equilibration, according to the previous study (Kim et al. 2020a). The correct concentration for Cs adsorption was established using CEC,  $Q_{\max}$ , and RIP tests. After separation, the Cs-adsorbed clays were centrifuged twice and resuspended in deionized water before drying at 70 °C for 24 h. ICP-MS was used to measure the Cs concentration in the aqueous phase, and the amount of Cs adsorbed onto the clays was 3.041 mg/g (= 22.86 mmol of Cs/kg clay) for illite, 3.896 mg/g (= 29.29 mmol of Cs/kg clay) for hydrobiotite, and 3.968 mg/g (= 29.83 mmol of Cs/kg clay) for montmorillonite.

To facilitate desorption, 0.35 g of Cs clays were combined with 1.0 M NaCl and 1.0 M oxalic acid solution (35 mL) in a polypropylene tube. The reaction was performed over two days in a shaking bath at 25 °C. The solid and liquid were separated through centrifugation, and the obtained supernatant was passed through a PVDF membrane filter (0.2- $\mu\text{m}$  pore size). The amount of Cs desorbed from the clay was calculated using ICP-MS.

### XRD analysis

To prepare the samples for X-ray diffraction (XRD) studies, the solid and liquid phases were separated via centrifugation. The solid was then dried at 60 °C to remove water before being ground into small particles using a mortar and pestle. The constituent mineral and basal spacing of the clay minerals was measured using XRD. XRD patterns of montmorillonite, hydrobiotite, and illite exposed to Cs-adsorbed, RIP, NaCl-treated, and oxalic acid-treated samples were analyzed. A step size of 0.02° at 2 s/step and in the range of  $2\theta = 2\text{--}30^\circ$  was used to acquire the data. The  $d$ -spacing of each clay mineral was analyzed using the Bragg equation ( $n\lambda = 2d\sin\theta$ ).

### EXAFS measurements and analysis

Cs L<sup>III</sup>-edge EXAFS spectra were obtained using a Si (111) double-crystal monochromator and two mirrors at the beamline (10C) of the Pohang Light Source (PLS, Pohang, Korea). The energy at the L<sup>III</sup>-edge of Cs was obtained through energy calibration in the transmission mode using a Cs solid standard diluted with boron nitride. The spectra were measured using Ge semiconductor detectors, and analyses were performed using REX2000 and FEFF 7.0. The radial structural function (RSF) was obtained from the Fourier transform of the  $k^3x(k)$  EXAFS function calculated in the range of 2.5–6.5 after subtracting the background of the original spectra. The phase-shift functions of Cs-O and Cs-Si were derived from the structural properties of Cs-OH and phyllosilicate ( $\text{Cs}_2\text{Si}_2\text{O}_5$ ) (Fan et al. 2012). A goodness-of-fit parameter, the residual factor ( $R_f$ , %), was determined to verify the fitting accuracy.

$$R_f = \sum \frac{\{k^3x_{\text{obs}}(k) - k^3x_{\text{cal}}(k)\}^2}{\{k^3x_{\text{obs}}(k)\}^2} \quad (9)$$

where  $x_{\text{obs}}(k)$  and  $x_{\text{cal}}(k)$  are the experimental and calculated absorption coefficients, respectively, at a given  $k(\text{\AA}^{-1})$ .

## Results and discussion

### Characteristics of Cs sorption on clay minerals

XRD analysis was performed to identify the interlayer structures of the clay minerals (Fig. S1). Each clay mineral sample displayed a distinctive XRD pattern (Park et al. 2019b), and montmorillonite and illite exhibited distinctive peaks at  $2\theta = 6.1^\circ$  and  $8.8^\circ$ , respectively. The XRD pattern of a mixed-layer clay mineral with expandable

vermiculite and non-expandable mica was visible in the hydrobiotite sample. A hydrobiotite peak was seen at  $2\theta = 7.4^\circ$ , while vermiculite and mica peaks were seen at  $2\theta = 8.8^\circ$  and  $6.1^\circ$ , respectively (Kim et al. 2017). Illite peaks were observed at  $8.7^\circ$ ,  $17.7^\circ$ , and  $26.5^\circ$ .

X-ray fluorescence (XRF) measurements were performed to analyze the elemental concentrations of the samples (Table S1). Because Si is a key component of quartz and phyllosilicate clay minerals, nearly all the samples contained it. The exchangeable interlayer cation Ca was present in the montmorillonite (SAz-1), which had a high Ca concentration (CaO = 6.8%). Similar to the illite sample, which contained K as an interlayer cation, a high K content was detected (K<sub>2</sub>O = 5.9%). Mg and K were the interlayer cations of vermiculite and biotite, respectively, and were prevalent in the hydrobiotite sample, which was composed of layers of mixed vermiculite and biotite. The hydrobiotite sample displayed a high Fe content because the trioctahedral layers of the biotite were composed of Mg and Fe.

The effects of the different clay minerals on the selective adsorption of Cs from the soil were determined using the CEC and RIP. The CECs of illite, hydrobiotite, and montmorillonite were 0.19, 0.99, and 1.33 meq/g, respectively, with the high CECs of montmorillonite and hydrobiotite being attributed to the presence of many interlayers, which led to ion exchange. RIP analysis revealed the FES content in the clay minerals. The RIPs of illite, hydrobiotite, and montmorillonite were 1.91  $\mu\text{mol/g}$ , 5.86  $\mu\text{mol/g}$ , and 4.23  $\mu\text{mol/g}$ , corresponding to CECs of 1.004%, 0.5920%, and 0.3181%, respectively (Table 1). These results suggest that, despite its lower CEC, illite may have a higher RIP/CEC fraction for Cs compared to montmorillonite and hydrobiotite, which agrees with previous results (Lee et al. 2017). In a previous study (Kwon et al. 2023), illite exhibited a low Cs adsorption capacity but high selectivity, whereas montmorillonite exhibited relatively low selectivity but high capacity. RIP has been proposed for estimating the number of Cs-selective adsorption sites for FESs in clay minerals by analyzing selective adsorption in the presence of competing ions, such as Ca<sup>2+</sup> and K<sup>+</sup>, excluding the adsorption at planar and ion-exchange sites (Absalom et al. 1999; Akemoto et al. 2021; De Koning et al. 2007; Durrant et al. 2018).

## Cs adsorption kinetic of clay minerals

Figure 2 depicts the kinetic model fits for the illite, hydrobiotite, and montmorillonite, and Table 2 presents the model-fitting parameters obtained using pseudo-first-order and pseudo-second-order kinetic models. Notably, the pseudo-second-order kinetic model exhibits higher  $R^2$  values, suggesting that this model best describes the adsorption data for all the clay minerals. Interestingly, the results reveal a faster rate constant for illite compared to hydrobiotite and montmorillonite (Table 2). Previous investigations have shown that the adsorption data are consistent with the pseudo-second-order kinetic model throughout the sorption period, thereby confirming the assumption for the model that the adsorption is due to chemisorption (Ho 2006; Kumar et al. 2005; Lalhriatpua et al. 2014). Furthermore, a previous study reported that the suitability of the pseudo-second-order kinetic model implies chemisorption as the main process governing the interactions at the solid/solution interface (Ho 2006).

Fig. S2 illustrates the variation of Cs adsorption over  $t^{1/2}$  for different types of clays. As seen from Fig. S2, Cs adsorption on the clays occurred in two phases: first, within the first 10 min, there was a rapid adsorption phase in which more than 50% of the metal ions rapidly bound to the adsorption sites of the clays (Supplementary Material). Subsequently, in the second phase, Cs ions gradually diffused into the clay pores. However, it is noteworthy that intraparticle diffusion alone does not fully govern the removal process, as the plots did not pass through the origin in Fig. S2 (Supplementary Material). This may be due to differences in mass transfer rates between the early and final stages of sorption (Önal et al. 2006).

## Cs adsorption isotherm of clay minerals

We evaluated the Cs sorption properties of illite, hydrobiotite, and montmorillonite using adsorption isotherms at 25 °C (Fig. 3). The highest amounts of Cs adsorption were  $0.9893 \pm 0.0158$  mmol/g (131.58 mg/g),  $0.4108 \pm 0.0128$  mmol/g (54.64 mg/g), and  $0.0883 \pm 0.0120$  mmol/g (11.74 mg/g) for montmorillonite, hydrobiotite, and illite, respectively. Montmorillonite had a much higher Cs adsorption capacity than illite and

**Table 1** Cation exchange capacity and Cs adsorbed onto illite, hydrobiotite, and montmorillonite

Clay	CEC (meq·g <sup>-1</sup> )	$Q_{\text{max}}$ (mmol·g <sup>-1</sup> )	RIP (μmol·g <sup>-1</sup> )	Cs adsorbed (mmol·g <sup>-1</sup> ) <sup>1)</sup>	RIP/CEC (%)	RIP/Cs adsorbed (%)
Illite	0.19	0.08568	1.909	0.02286	1.004	8.35
Hydrobiotite	0.99	0.56	5.8609	0.02986	0.5920	19.63
Montmorillonite	1.33	0.88	4.2301	0.02983	0.3181	14.10

<sup>1)</sup>Amount of Cs used for the desorption test

**Fig. 2** Kinetics of Cs adsorption by illite, hydrobiotite, and montmorillonite (initial Cs concentration = 3.7594 mmol/L (500 mg/L), contact time = 24 h, clay dosage = 2 g/L, shaking speed = 150 rpm, pH = 6, and temperature = 25 °C). The solid lines indicate the obtained pseudo-second-order kinetic curves

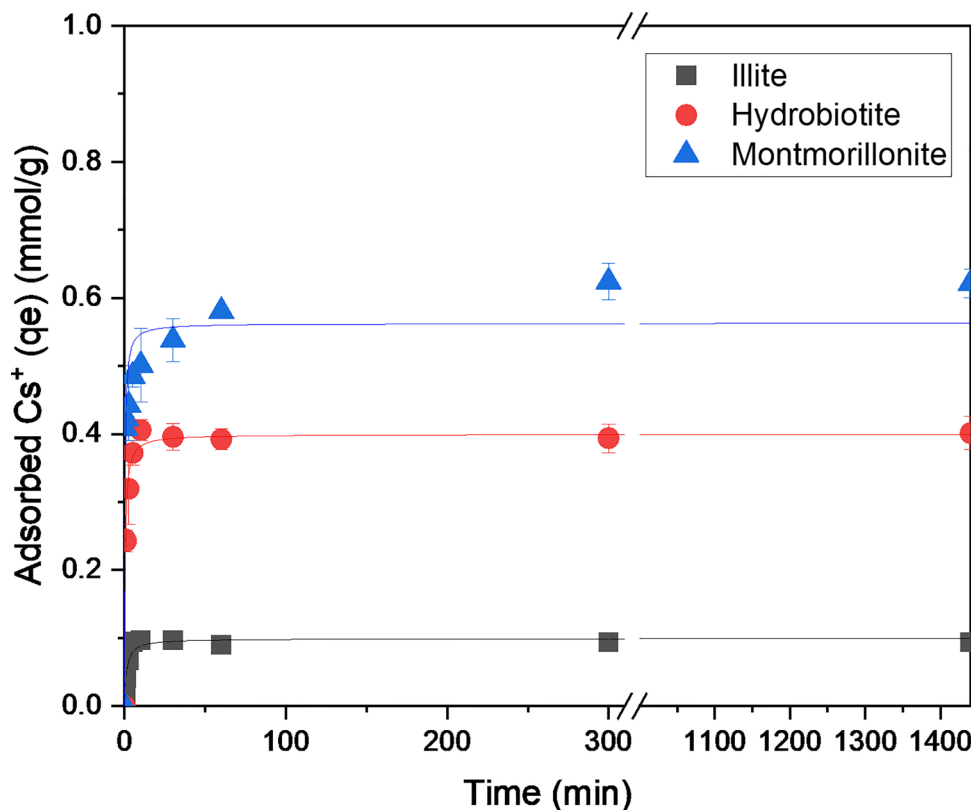


**Table 2** Estimated kinetic model parameters for Cs adsorption on clay minerals

Model	Parameter	Sample		
		Illite	Hydrobiotite	Montmorillonite
Pseudo-first-order	$q_e$ (mmol/g)	0.0545	0.1036	0.1927
	$k_1$ (/min)	0.0336	0.0401	0.0203
	$R^2$	0.8679	0.7014	0.9076
Pseudo-second-order	$q_e$ (mmol/g)	0.0990	0.3992	0.5624
	$k_2$ (mmol/mg·min)	8.0966	5.6245	6.1701
	$R^2$	0.9533	0.9777	0.9347

hydrobiotite because of its high CEC (Schnurr et al. 2015; Yu et al. 2016) whereas illite had the lowest Cs adsorption capacity because of the limited interlayer exchange of  $K^+$  ions. These results confirm that several sites contribute to Cs adsorption onto clay minerals (Ikhsan et al. 2005; Motokawa et al. 2014). The highest Cs amounts of 112.19 mg/g and 8.35 mg/g for Ca-montmorillonite and illite, respectively, obtained in this study are consistent with Kwon et al. (2023), while the highest Cs amount of 64.0 mg/g for hydrobiotite agrees with Akemoto et al. (2021).

Table 3 presents a summary of the parameters with the five isotherm adsorption models used in this study. Comparing the correlation coefficients ( $R^2$ ), the results are as follows: Sips (0.9449–0.9950) > Redlich-Peterson (0.8530–0.9917) > Langmuir (0.9089–0.9797) > Freundlich (0.9197–0.9545) > Dubinin-Radushkevich

(0.5509–0.9598). Notably, the Sips isotherm model shows the best agreement for illite and montmorillonite, whereas the Redlich-Peterson isotherm model shows the best agreement for hydrobiotite. The three-parameter isotherms for Redlich-Peterson and Sips combine the Freundlich and Langmuir models, which have high  $R^2$  values ( $R^2 > 0.9449$ ). The Sips and Redlich-Peterson isotherm constants  $1/n$  and  $g$  are close to 1, indicating that both isotherm models are close to the Langmuir isotherm. The Langmuir model with the analysis of all isotherm parameters provides a better description of the sorption process than the other models, and Cs adsorption on the clays proceeds via a homogeneous monolayer adsorption mechanism (Palansooriya et al. 2022; Redlich & Peterson 1959). Within the Langmuir model, the  $R_L$  value indicates the shape and nature of the isotherm as linear ( $R_L = 1$ ),

**Fig. 3** Cs adsorption isotherms obtained from (a) illite, (b) hydrobiotite, and (c) montmorillonite clay samples at 25 °C (initial Cs concentration = 0.1503–6.0150 mmol/L, contact time = 24 h, clay dosage = 2 g/L, shaking speed = 150 rpm, pH = 6, and temperature = 25 °C). The solid lines indicate Sips isotherm curves for illite and montmorillonite, and Redlich-Peterson isotherms curves for hydrobiotite

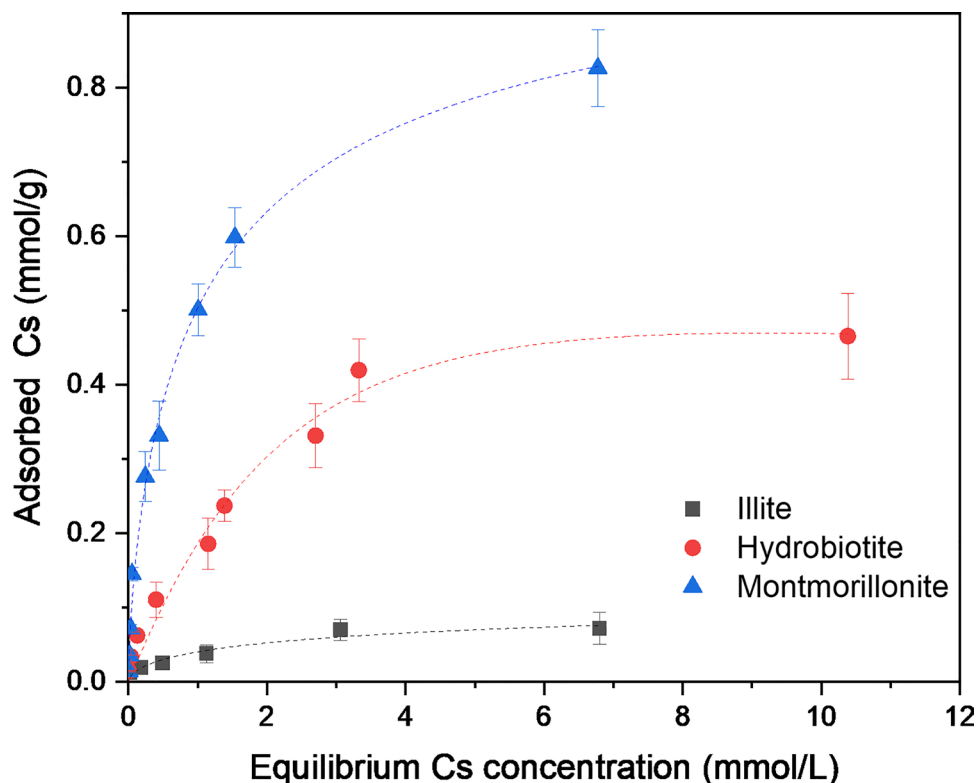


**Table 3** Estimated adsorption isotherm model parameters for Cs adsorption onto illite, hydrobiotite, and montmorillonite

Model	Parameter	Sample		
		Illite	Hydrobiotite	Montmorillonite
Freundlich	$K_F$ (mmol/g)/(mmol/L) <sup>1/n</sup>	0.0396	0.1814	0.4428
	1/n	0.3186	0.5002	0.3606
	$R^2$	0.9357	0.9783	0.9602
Dubinin-Radushkevich	$q_D$ (mmol/g)	0.0453	0.2369	0.5339
	$K_{DR}$ (mol <sup>2</sup> /J <sup>2</sup> )	$1.7299 \times 10^{-8}$	$2.0160 \times 10^{-8}$	$2.5347 \times 10^{-8}$
	$E$ (kJ/mol)	7.6030	7.0429	6.2811
	$R^2$	0.6407	0.8018	0.9648
Langmuir	$Q_{max}$ (mmol/g)	0.0857	0.5647	0.8795
	$K_L$ (L/mmol)	0.9484	0.5601	1.5217
	$R^2$	0.9271	0.9744	0.9822
Sips	$q_m$ (mg/g)	0.1338	0.5707	1.0725
	$K_s$ (L/mmol)	0.4315	0.5538	0.8846
	1/n	0.5798	0.9788	0.7038
	$R^2$	0.9449	0.9744	0.9950
Redlich-Peterson	$K_R$ (L/mol)	0.0867	0.2214	2.9412
	$\alpha R$ (L/mmol)	1.0000	0.1874	4.9030
	$g$	0.9655	1.2975	0.8056
	$R^2$	0.9118	0.9787	0.9938

irreversible ( $R_L = 0$ ), unfavorable ( $R_L > 1$ ), and favorable ( $0 < R_L < 1$ ). The calculated  $R_L$  values in the range from 0.1849 to 0.2289 correspond to favorable adsorption in Cs adsorption by clays (Fu et al. 2023).

### Cs desorption from by NaCl clay minerals

Desorption experiments were performed by adjusting the amount of Cs below 20% of the RIP value to evaluate the

desorption efficiency for planar sites, interlayers, and RIP (Table 1). We analyzed the efficiency of Cs desorption from illite, hydrobiotite, and montmorillonite using different desorbents, including NaCl and oxalic acid, owing to their ion exchange and strong acid-chelating properties. When 1.0 M NaCl was used as the desorbent, illite showed a higher Cs desorption efficiency (74.32%) than hydrobiotite (45.53%) and montmorillonite (30.34%) (Fig. 4). For hydrobiotite, 45.5% (0.01334 mmol/g) of Cs was adsorbed in an ion-exchangeable form on the surface sites and 54.4% (0.01595 mmol/g) of the Cs remained in the clay (Fig. 4). For montmorillonite, 30.3% (0.00905 mmol/g) of the Cs was adsorbed in an ion-exchangeable form on the surface sites and 69.7% (0.02078 mmol/g) of Cs remained in the clay. In contrast, 74% (0.01699 mmol/g) of the Cs in illite was in the ion-exchangeable form, while 25.7% (0.00587 mmol/g) remained in the clay (Fig. 4).

NaCl is used to extract the ion-exchangeable form of Cs from clay minerals (Dzene et al. 2015), and the amount of Cs desorbed using NaCl indicated the ion-exchangeable form of Cs in the clay minerals. Montmorillonite and hydrobiotite showed significant interlayer and RIP contributions to the overall Cs adsorption (Park et al. 2021b). Based on these results, it was difficult to desorb montmorillonite using cations. In a previous study,  $\text{Na}^+$  ions exhibited the highest desorption rate (40%), contrary to expectations, as they became more dispersible owing to an increase in the tactoid content (Fukushi et al. 2014), and the efficiency in our study was 30%. A previous study showed efficient desorption of 40% for hydrobiotite using ammonium ions (Park et al. 2021a),

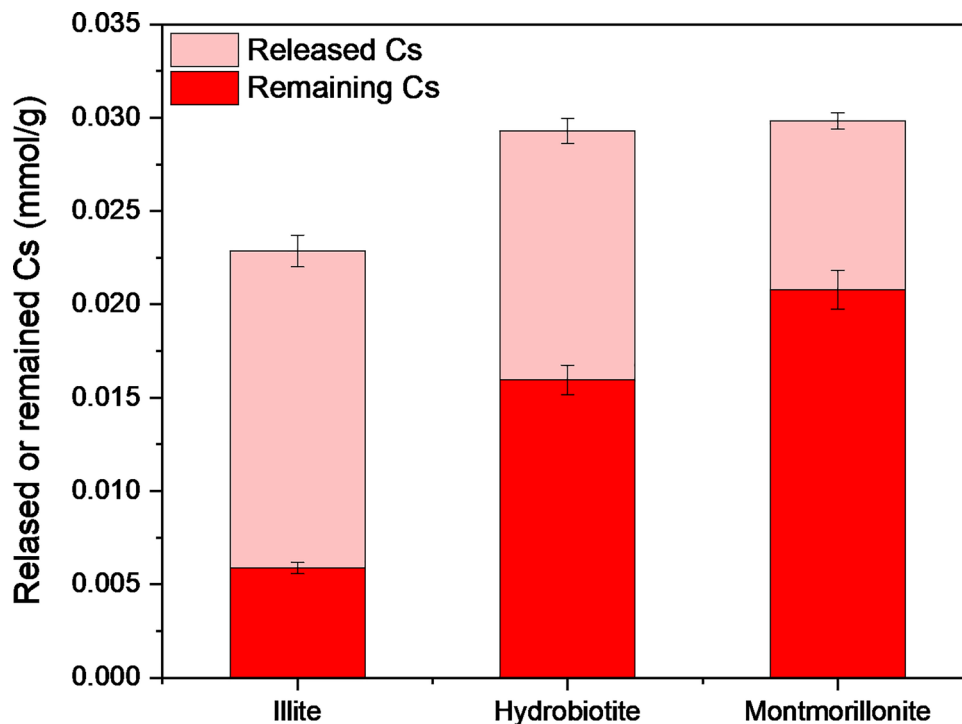
which is identical to our desorption efficiency (40%). Similar IS complexes were produced by Cs adsorbed on the interlayers and FESs (Fan et al. 2014b), indicating low desorption efficiency. Illite clay minerals have highly Cs-selective adsorption sites, such as FESs and type II sites (Bradbury & Baeyens 2000), and exchange between the Cs ions adsorbed onto these sites and other cations is limited (de Koning & Comans 2004; Fuller et al. 2015). The contents of type I (FESs) and type II sites in illite are typically less than 0.25% and 20% of the CEC, respectively (Bradbury & Baeyens 2000). In this study, approximately 26% of the CEC in the illite was expected to be strongly bound to Cs ions, which are not easily exchanged using desorption agents.

### XRD analysis

After the desorption of NaCl and oxalic acid from the Cs clays, XRD was employed to characterize the interlayer distances of these clay minerals and explore the structural alterations of montmorillonite, hydrobiotite, and illite under various experimental conditions (Fig. 5). The interlayer distance for 2:1 phyllosilicates can be determined using Bragg's law by the 2-theta value. The initial diffraction peak in the XRD pattern is typically assigned to the first-order diffraction of the 001 facet (Wu et al. 2018, 2015).

Characteristic peaks at  $8.7^\circ$ ,  $17.7^\circ$ , and  $26.5^\circ$  were observed for illite, with no significant changes observed in the Cs adsorption, RIP, NaCl, and oxalic acid desorption samples. Illite, a non-expansive clay mineral, displayed a consistent  $d$ -spacing of 10.0 Å ( $8.7^\circ$ ) in both the dry and

**Fig. 4** Cs desorption efficiency with 1 M NaCl desorption agents for illite, hydrobiotite, and montmorillonite (amount of Cs adsorbed onto the clays (22.86 mmol of Cs/kg for illite, 29.29 mmol of Cs/kg for hydrobiotite, and 29.83 mmol of Cs/kg for montmorillonite), contact time = 24 h, solid to liquid (S/L) ratio of 1:100, shaking speed = 150 rpm, and temperature = 25 °C)





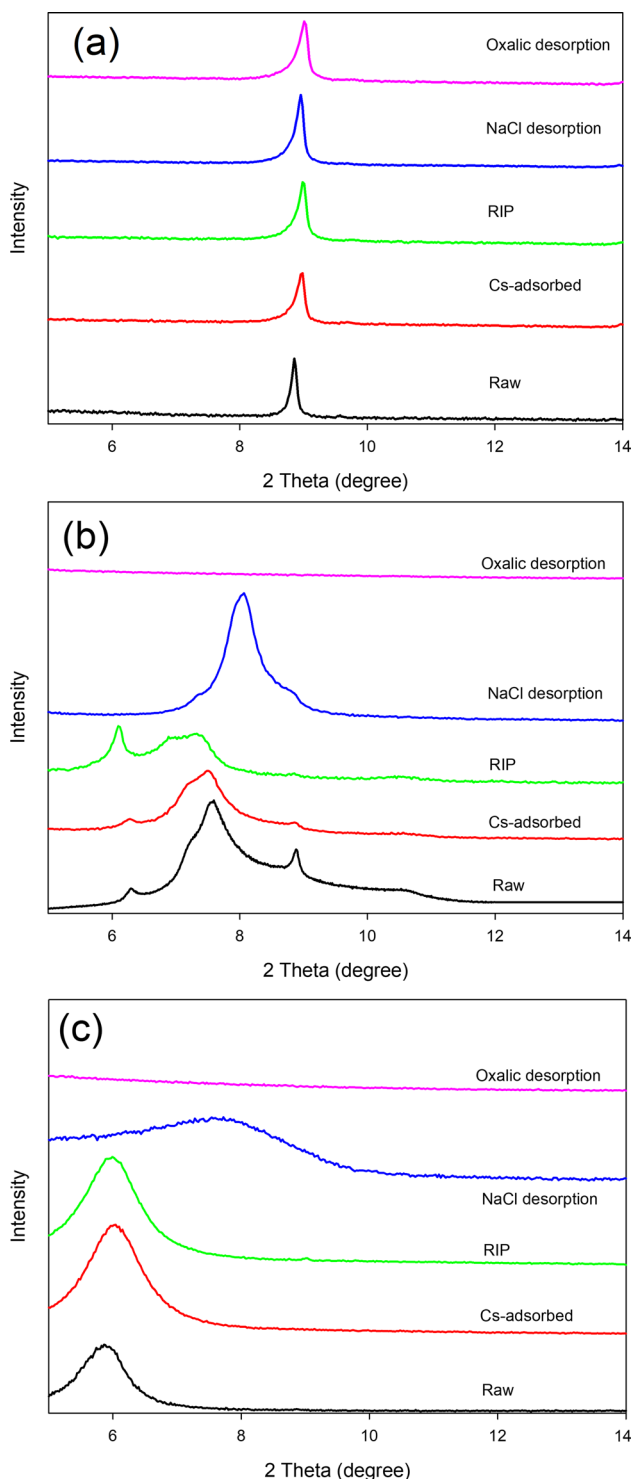


**Fig. 5** XRD analysis for illite, hydrobiotite, and montmorillonite for adsorption, RIP, NaCl, and oxalic acid desorption

wet stages, demonstrating that its crystal structure was unaffected by the Cs adsorbed onto it in the adsorption, RIP, NaCl, and oxalic desorption samples (Fig. 5a). This indicated that cation exchange was the primary mechanism

by which Cs was adsorbed onto the planar surfaces (Okumura et al. 2014). A small amount of Cs can be irreversibly adsorbed onto FESs, although it is adsorbed onto planar sites and does not change the structure of illite (Kim et al. 1996a). Furthermore, Cs adsorbed onto the FESs can migrate into the illite interlayer and become fixed in the interlayer along with the FESs (Fuller et al. 2015; Park et al. 2019b).

As shown in Fig. 5b, some diffraction peaks were observed in relation to the initial hydrobiotite. Interstratification, in which the structures of vermiculite [6.1° (14 Å)] and biotite [8.8° (10 Å)] are alternatively repeated, was attributed to reflection at approximately 7.4° (11.9 Å) (Kikuchi & Kogure 2018). This reflection was also observed in hydrobiotite. Therefore, it was determined that the hydrobiotite had basal spacings of 14 and 10 Å. After adsorption with Cs, the peak (14 Å) of vermiculite decreased when Cs entered the interlayers via ion exchange with  $Mg^{2+}$  (Kogure et al. 2012). In the RIP sample, the peak (14 Å) of vermiculite increased when  $Ca^{2+}$  entered the interlayer, suggesting that valent cations exhibit larger hydrous radii and greater ionic valences than monovalent cations, which can increase the expansion of the interlayer region. In contrast, NaCl desorption from Cs-hydrobiotite reduced the interlayer distance to 8° (11 Å), consistent with previous experimental findings (Han et al. 2023; Kwon et al. 2023). The XRD patterns demonstrate that the interlayer distance was decreased by the monovalent cations of  $Na^+$ . This peak disappeared in the case of oxalic acid.

Without alkaline cations, interlayer distances in montmorillonite normally range from 15 to 25 Å. Characteristic peaks at 6° (14.7 Å) were found in Ca-montmorillonite, with no significant changes observed in the raw Cs adsorption and RIP samples. For the NaCl-desorbed sample, the peak at 7.7° shifted to a higher angle. The collapse of the montmorillonite layer at different  $Na^+$  concentrations was demonstrated by XRD patterns after substituting  $Ca^{2+}$  with  $Na^+$  (Kwon et al. 2023). The collapse of the interlayer-fixed Cs tightly narrowed the interlayers of hydrobiotite and montmorillonite owing to the small ionic radius of the monovalent cation  $Na^+$  (Kwon et al. 2023). This peak disappeared in the case of oxalic acid owing to the dissolution of the layer. After NaCl treatment, XRD data showed the tightly narrowed hydrobiotite and montmorillonite interlayers owing to the monovalent cation  $Na^+$  against divalent cation  $Mg^{2+}$  or  $Ca^{2+}$ , resulting that the low desorption efficiency was due to the collapse of the interlayer-fixed Cs.

## EXAFS analysis

According to Liu et al. (2008), EXAFS data can be used to estimate the bond lengths of Cs-O couples in Cs-containing clay minerals. Bostick et al. (2002) found that the IS complexes between clay mineral siloxane groups and dehydrated

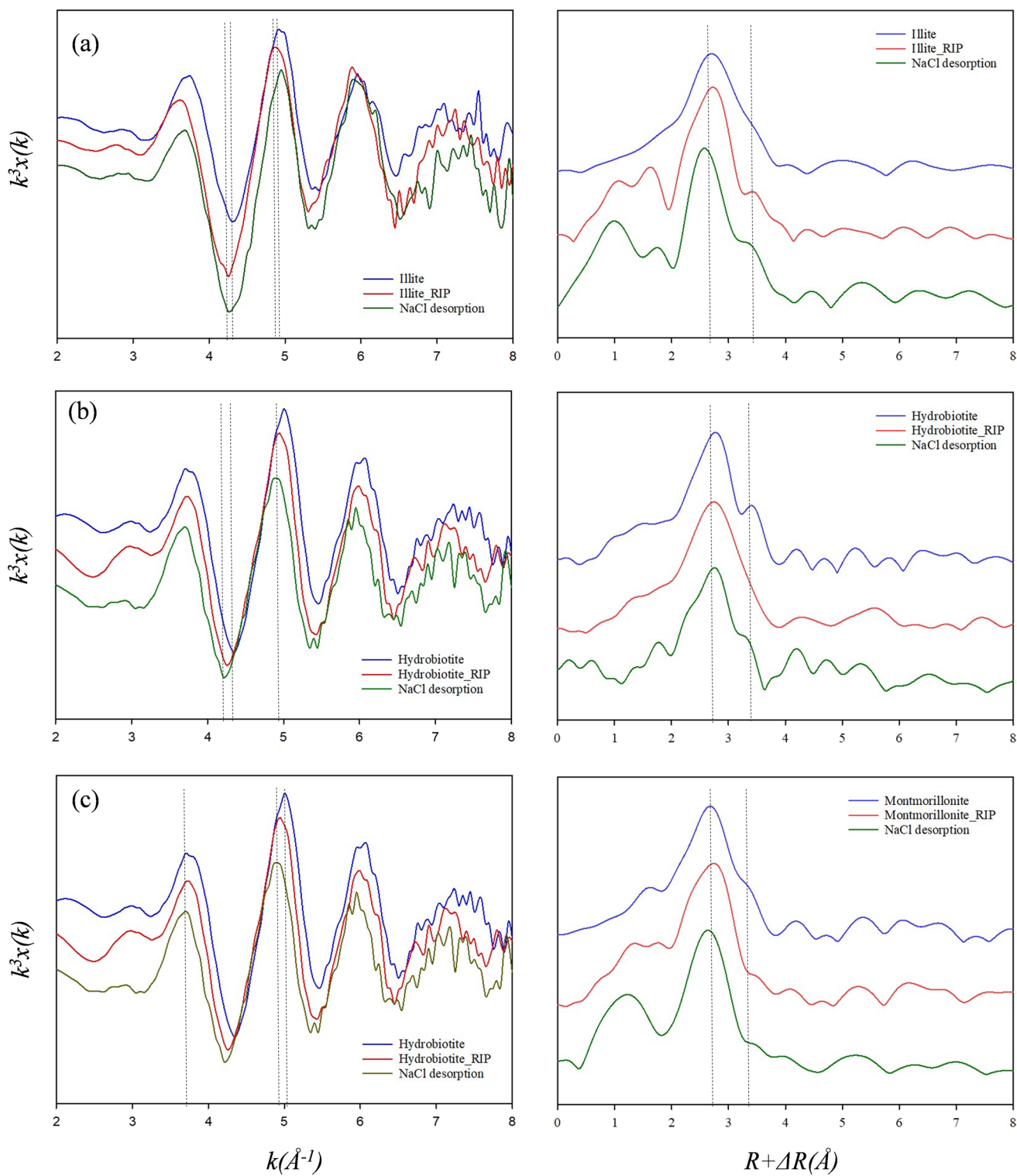


**Fig. 6** Cs LIII-edge EXAFS spectra for Cs adsorbed **a** illite, **b** hydrobiotite, and **c** montmorillonite for  $k^3$ -weighted  $x(k)$  oscillation and corresponding RSFs (phase-shift uncorrected)

Cs resulted in longer Cs-O bond distances. Figure 6 shows the Cs L<sup>3</sup>-edge EXAFS spectra of the clay samples for the Cs adsorption, RIP, and NaCl desorption processes. As shown in Fig. 6a, the  $k^3x(k)$  values of illite exhibited slightly different oscillation patterns compared with those of RIP and NaCl desorption. The Fourier transform of illite revealed the presence of a first coordination shell, corresponding to an OS Cs-O bonding range of 3.05–3.12 Å for Cs-adsorbed clay. Contrastingly, the RIP and NaCl desorption samples exhibited weak second-coordination shells ranging from 3.47 to 3.55 Å, indicating IS Cs-O bonding. These results suggest that desorption did not remove the partially bound Cs from illite, likely because FESs were present.

Similarly, the  $k^3x(k)$  values of the hydrobiotite and montmorillonite samples displayed slightly different oscillation patterns compared with those of RIP and NaCl desorption. Although the NaCl desorption of hydrobiotite showed a weak second-coordination shell, indicating IS Cs-O bonding, the NaCl desorption of montmorillonite did not exhibit a distinct second-coordination shell, suggesting that the location of Cs in montmorillonite is primarily determined by the inherent interlayer ion exchange of clay minerals, rather than being influenced by FESs. Additionally, the partially bound IS coordination signifying partial bonding was presumed to have been removed mainly by desorption. This result agrees with Park et al. (2019b). Although the interlayer collapsed due to the presence of

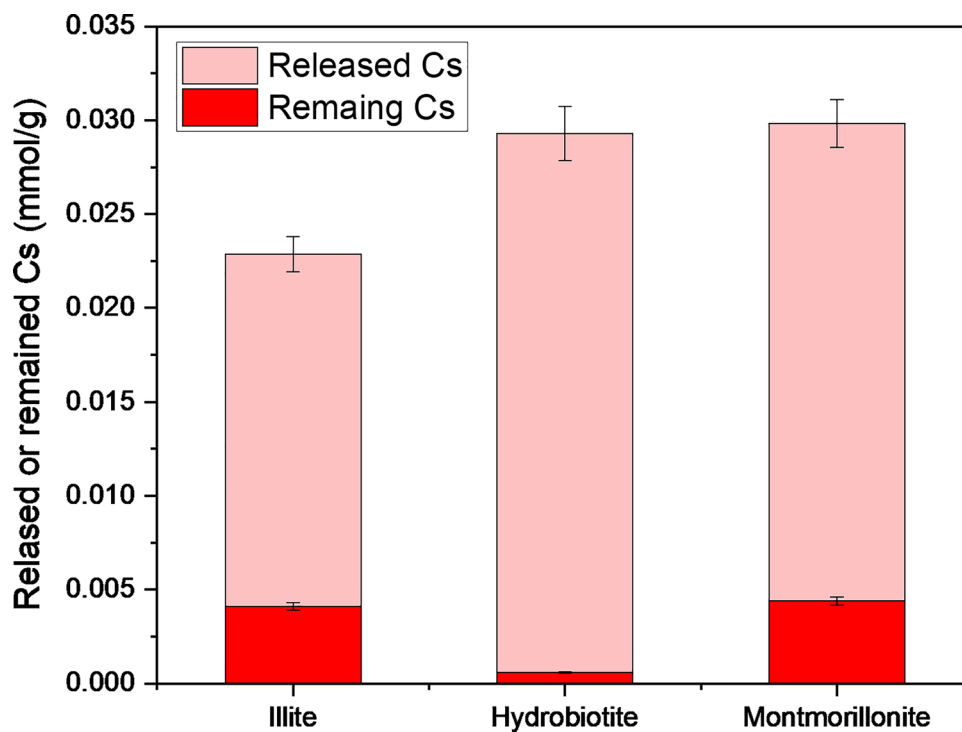
Cs on montmorillonite, IS complexes were still observed in the hydrobiotite. The fixation of Cs in the interlayer space is indicated by an irreversible reduction in basal spacing in montmorillonite (Iijima et al. 2010). However, EXAFS fitting has demonstrated that the fixation is not an IS complexation. The basal spacing in the hydrobiotite decreased to 1.09 nm, which is similar to that in illite (1.07 nm) (Fuller et al. 2015). The results indicate that the basal spacing and Cs-O distance are evidence of IS complexation of Cs in the clay mineral.

In the case of illite without an interlayer, ion exchangers such as NaCl readily removed Cs from the planar sites; however, FESs and type II sites were not readily removed because of strong IS bonding. Contrastingly, hydrobiotite and montmorillonite shrank the interlayer after NaCl desorption, hindering Cs desorption. In hydrobiotite, the vermiculite and biotite layers became illite-like after NaCl desorption. These results suggest that ion exchange in the interlayers of hydrobiotite and montmorillonite is limited because of their contraction due to NaCl desorption, as shown by the XRD and EXAFS analyses.

### Chelation desorption by oxalic acid for Cs from clay minerals

Unlike NaCl desorption, which cause only ion exchange, oxalic acid can ion exchange with Cs, dissolve metal components in clay minerals, and disrupt mineral structures

**Fig. 7** Cs desorption efficiency with 1 M oxalic acid for illite, hydrobioite, and montmorillonite (Amount of Cs adsorbed onto the clays (22.86 mmol of Cs/kg for illite, 29.29 mmol of Cs/kg for hydrobiotite, and 29.83 mmol of Cs/kg for montmorillonite), contact time = 24 h, solid to liquid (S/L) ratio of 1:100, shaking speed = 150 rpm, and temperature = 25 °C)



(Carroll & Starkey 1971; Komadel et al. 1996; Van Rompaey et al. 2002). When oxalic acid was used as a desorbent, hydrobiotite had the highest Cs desorption efficiency (98%), followed by montmorillonite (85.26%) and illite (82%) (Fig. 7). Hydrobiotite has a high Fe and Mg content (Table S1); therefore, its structure could be destroyed by the chelating effect, resulting in more than 98% of the Cs being desorbed (Kim et al. 2020b), probably due to the co-desorption of Cs with other constituents during leaching. In montmorillonite and illite, the desorption rate of oxalic acid was lower because the amount adsorbed by the FES or interlayer was not well desorbed. Although Cs desorption from a collapsed interlayer is difficult, chelation can be effective.

Oxalic acid removed the FES or the interlayer by dissolving cations, demonstrating that it is effective against FES and the hydrobiotite interlayer by dissolving mineral components such as Fe and Mg. Therefore, chelation or strong acids are required to alter the structure by eluting other cations to remove Cs from clay minerals. This study provides the environmental benefit of understanding the role of interlayers for Cs adsorption/desorption in clays and selecting the effective desorbent for Cs in clays.

## Conclusions

Illite, hydrobiotite, and montmorillonite exhibited different sorption behaviors and RIP values for Cs. Illite had a higher affinity for Cs than hydrobiotite and montmorillonite because of the presence of selective FESs. The highest Cs sorption was observed for montmorillonite, followed by hydrobiotite and illite. The adsorption kinetic and isotherm results showed that the Cs adsorption on clay minerals fitted well with the pseudo-second-order model and the Sips and Redlich-Peterson adsorption model, indicating that Cs adsorption follows chemisorption and homogeneous monolayer adsorption mechanism. The XRD patterns of illite, hydrobiotite, and montmorillonite after Cs adsorption and desorption showed that Cs adsorption did not significantly affect the structure of illite. In contrast, hydrobiotite and montmorillonite showed shrinkage of their interlayer distances after NaCl desorption due to the small ionic radius of  $\text{Na}^+$  ions. XRD and EXAFS analyses confirmed the tightly narrowed interlayer of montmorillonite and hydrobiotite and IS bonds of hydrobiotite. EXAFS analysis revealed interlayer bonding in illite and hydrobiotite. It is difficult to use ion exchange or FESs to remove Cs from shrunken interlayers. To effectively remove Cs, oxalic acid, which has a chelating effect, should be used to dissolve the interlayer. Therefore, research on the interlayer changes during adsorption and desorption could provide important insights for improving decontamination efficiency and understanding the behavior of Cs in clay.

**Supplementary Information** The online version contains supplementary material available at <https://doi.org/10.1007/s11356-024-32826-9>.

**Author contribution** All authors contributed to the study's conception and design. In-Ho Yoon is responsible for writing—original draft, conceptualization, methodology, software, data curation, visualization, and supervision. Sang-Ho Lee is assigned to the investigation, data curation, and writing—original draft. Ilgook Kim is responsible for the writing—review and editing, and validation. Sung Man Kim did the methodology, investigation, and data curation. All authors read and approved the final manuscript.

**Funding** This study was supported by grants from the National Research Foundation of Korea (NRF), funded by the Korean government, Ministry of Science, ICT and Future Planning (RS-2023-00243600 and 2022M2D2A1A02063569).

**Data availability** Data and materials can be made available on request.

## Declarations

**Ethics approval** Not applicable.

**Consent to participate** Not applicable.

**Consent for publication** Not applicable.

**Competing interests** The authors declare no competing interests.

## References

- Abollino O, Giacomino A, Malandrino M, Mentasti E (2008) Interaction of metal ions with montmorillonite and vermiculite. *Appl Clay Sci* 38:227–236
- Absalom J, Young S, Crout N, Nisbet A, Woodman R, Smolders E, Gillett A (1999) Predicting soil to plant transfer of radiocesium using soil characteristics. *Environ Sci Technol* 33:1218–1223
- Akemoto Y, Sakti SCW, Kan M, Tanaka S (2021) Interpretation of the interaction between cesium ion and some clay minerals based on their structural features. *Environ Sci Pollut Res* 28:14121–14130
- Bostick BC, Vairavamurthy MA, Karthikeyan K, Chorover J (2002) Cesium adsorption on clay minerals: an EXAFS spectroscopic investigation. *Environ Sci Technol* 36:2670–2676
- Bourg IC, Sposito G, Bourg AC (2007) Modeling cation diffusion in compacted water-saturated sodium bentonite at low ionic strength. *Environ Sci Technol* 41:8118–8122
- Bradbury MH, Baeyens B (2000) A generalised sorption model for the concentration dependent uptake of caesium by argillaceous rocks. *J Contam Hydrol* 42:141–163
- Carroll D, Starkey HC (1971) Reactivity of clay minerals with acids and alkalies. *Clays Clay Miner* 19:321–333
- Chen L, Dong Y (2013) Sorption of  $^{63}\text{Ni}$  (II) to montmorillonite as a function of pH, ionic strength, foreign ions and humic substances. *J Radioanal Nucl Chem* 295:2117–2123
- Cornell R (1993) Adsorption of cesium on minerals: a review. *J Radioanal Nucl Chem* 171:483–500
- de Koning A, Comans RN (2004) Reversibility of radiocaesium sorption on illite. *Geochim Cosmochim Acta* 68:2815–2823
- De Koning A, Konoplev A, Comans R (2007) Measuring the specific caesium sorption capacity of soils, sediments and clay minerals. *Appl Geochem* 22:219–229

- Ding D, Zhang Z, Lei Z, Yang Y, Cai T (2016) Remediation of radiocesium-contaminated liquid waste, soil, and ash: a mini review since the Fukushima Daiichi Nuclear Power Plant accident. *Environ Sci Pollut Res* 23:2249–2263
- Durrant CB, Begg JD, Kersting AB, Zavarin M (2018) Cesium sorption reversibility and kinetics on illite, montmorillonite, and kaolinite. *Sci Total Environ* 610:511–520
- Dzene L, Tertre E, Hubert F, Ferrage E (2015) Nature of the sites involved in the process of cesium desorption from vermiculite. *J Colloid Interface Sci* 455:254–260
- Fan Q, Xu J, Niu Z, Li P, Wu W (2012) Investigation of Cs (I) uptake on Beishan soil combined batch and EDS techniques. *Appl Radiat Isot* 70:13–19
- Fan Q, Tanaka M, Tanaka K, Sakaguchi A, Takahashi Y (2014a) An EXAFS study on the effects of natural organic matter and the expandability of clay minerals on cesium adsorption and mobility. *Geochim Cosmochim Acta* 135:49–65
- Fan Q, Yamaguchi N, Tanaka M, Tsukada H, Takahashi Y (2014b) Relationship between the adsorption species of cesium and radiocesium interception potential in soils and minerals: an EXAFS study. *J Environ Radioact* 138:92–100
- Fu C, Tan Z, Cheng J, Xie J, Dai X, Du Y, Zhu S, Wang S, Yan M (2023) Effective removal of cesium by ammonium molybdophosphate–polyethylene glycol magnetic nanoparticles. *J Environ Chem Eng* 11:110544
- Fukushi K, Sakai H, Itono T, Tamura A, Arai S (2014) Desorption of intrinsic cesium from smectite: inhibitive effects of clay particle organization on cesium desorption. *Environ Sci Technol* 48:10743–10749
- Fuller AJ, Shaw S, Ward MB, Haigh SJ, Mosselmans JFW, Peacock CL, Stackhouse S, Dent AJ, Trivedi D, Burke IT (2015) Caesium incorporation and retention in illite interlayers. *Appl Clay Sci* 108:128–134
- Han B, Zhang X, Liu C, Ma G, Guo D, Shao Y, Li P, Liang J, Fan Q (2023) Essential role of the interlayer of montmorillonite, vermiculite, and illite for Ni (II) sorption. *J Radioanal Nucl Chem* 332:1315–1323
- Ho Y-S (2006) Review of second-order models for adsorption systems. *J Hazard Mater* 136:681–689
- Hwang J, Han WS, Choung S, Kim J-W, Suk H, Lee J (2023) Diverse sorption capacities and contribution of multiple sorptive sites on illitic clays to assess the immobilization of dissolved cesium in subsurface environments. *J Hazard Mater* 441:129973
- Iijima K, Tomura T, Shoji Y (2010) Reversibility and modeling of adsorption behavior of cesium ions on colloidal montmorillonite particles. *Appl Clay Sci* 49:262–268
- Ikhsan J, Wells JD, Johnson BB, Angove MJ (2005) Surface complexation modeling of the sorption of Zn (II) by montmorillonite. *Colloids Surf Physicochem Eng Aspects* 252:33–41
- Kikuchi R, Kogure T (2018) Structural and compositional variances in 'hydrobiotite' sample from Palabora, South Africa. *Clay Science* 22:39–52
- Kim BH, Park CW, Yang H-M, Seo B-K, Lee B-S, Lee K-W, Park SJ (2017) Comparison of Cs desorption from hydrobiotite by cationic polyelectrolyte and cationic surfactant. *Colloids Surf Physicochem Eng Aspects* 522:382–388
- Kim S-M, Yoon I-H, Kim I-G, Park CW, Sohn Y, Kim J-H, Park S-J (2020a) Cs desorption behavior during hydrothermal treatment of illite with oxalic acid. *Environ Sci Pollut Res* 27:35580–35590
- Kim S-M, Yoon I-H, Kim I, Kim J-H, Park S-J (2020b) Hydrothermal desorption of Cs with oxalic acid from hydrobiotite and wastewater treatment by chemical precipitation. *Energies* 13:3284
- Kim Y, Cygan RT, Kirkpatrick RJ (1996a) <sup>133</sup>Cs NMR and XPS investigation of cesium adsorbed on clay minerals and related phases. *Geochim Cosmochim Acta* 60:1041–1052
- Kim Y, Kirkpatrick RJ, Cygan RT (1996b) <sup>133</sup>Cs NMR study of cesium on the surfaces of kaolinite and illite. *Geochim Cosmochim Acta* 60:4059–4074
- Kogure T, Morimoto K, Tamura K, Sato H, Yamagishi A (2012) XRD and HRTEM evidence for fixation of cesium ions in vermiculite clay. *Chem Lett* 41:380–382
- Komadel P, Madejová J, Janek M, Gates WP, Kirkpatrick R, Stucki JW (1996) Dissolution of hectorite in inorganic acids. *Clays Clay Miner* 44:228–236
- Kumar KV, Ramamurthi V, Sivanesan S (2005) Modeling the mechanism involved during the sorption of methylene blue onto fly ash. *J Colloid Interface Sci* 284:14–21
- Kwon S, Lim J, Seoung D, Cho Y, Park B (2023) Comparative study of the cesium adsorption behavior of montmorillonite and illite based on their mineralogical properties and interlayer cations. *J Hazard Mater Adv* 10:100258
- Lalhriatpuia C, Tiwari D, Lee S-M (2014) Immobilized nickel hexacyanoferrate on activated carbons for efficient attenuation of radio toxic Cs (I) from aqueous solutions. *Appl Surf Sci* 321:275–282
- Lee J, Park S-M, Jeon E-K, Baek K (2017) Selective and irreversible adsorption mechanism of cesium on illite. *Appl Geochem* 85:188–193
- Liu X, Lu X, Wang R, Zhou H (2008) Effects of layer-charge distribution on the thermodynamic and microscopic properties of Cs-smectite. *Geochim Cosmochim Acta* 72:1837–1847
- Miranda-Trevino JC, Coles CA (2003) Kaolinite properties, structure and influence of metal retention on pH. *Appl Clay Sci* 23:133–139
- Motokawa R, Endo H, Yokoyama S, Nishitsuji S, Kobayashi T, Suzuki S, Yaita T (2014) Collective structural changes in vermiculite clay suspensions induced by cesium ions. *Sci Rep* 4:6585
- Mukai H, Hatta T, Kitazawa H, Yamada H, Yaita T, Kogure T (2014) Speciation of radioactive soil particles in the Fukushima contaminated area by IP autoradiography and microanalyses. *Environ Sci Technol* 48:13053–13059
- Nagy NM, Kónya J, Wazelischen-Kun G (1999) The adsorption and desorption of carrier-free radioactive isotopes on clay minerals and Hungarian soils. *Colloids Surf Physicochem Eng Aspects* 152:245–250
- Okumura M, Nakamura H, Machida M (2013) Mechanism of strong affinity of clay minerals to radioactive cesium: first-principles calculation study for adsorption of cesium at frayed edge sites in muscovite. *J Phys Soc Jpn* 82:033802
- Okumura T, Tamura K, Fujii E, Yamada H, Kogure T (2014) Direct observation of cesium at the interlayer region in phlogopite mica. *Microscopy* 63:65–72
- Önal Y, Akmil-Başar C, Eren D, Sarıcı-Özdemir Ç, Depci T (2006) Adsorption kinetics of malachite green onto activated carbon prepared from Tunçbilek lignite. *J Hazard Mater* 128:150–157
- Palansooriya KN, Yoon I-H, Kim S-M, Wang C-H, Kwon H, Lee S-H, Igalavithana AD, Mukhopadhyay R, Sarkar B, Ok YS (2022) Designer biochar with enhanced functionality for efficient removal of radioactive cesium and strontium from water. *Environ Res* 214:114072
- Park CW, Kim I, Yoon I-H, Yang H-M, Seo B-K (2021a) Behaviors of desorption agents during removal of Cs from clay minerals and actual soil. *J Nucl Fuel Cycle Waste Technol* 19:39–49
- Park CW, Kim S-M, Kim I, Yoon I-H, Hwang J, Kim J-H, Yang H-M, Seo BK (2021b) Sorption behavior of cesium on silt and clay soil fractions. *J Environ Radioact* 233:106592
- Park S-M, Alessi DS, Baek K (2019a) Selective adsorption and irreversible fixation behavior of cesium onto 2: 1 layered clay mineral: a mini review. *J Hazard Mater* 369:569–576
- Park S-M, Lee J, Jeon E-K, Kang S, Alam MS, Tsang DC, Alessi DS, Baek K (2019b) Adsorption characteristics of cesium on the clay minerals: structural change under wetting and drying condition. *Geoderma* 340:49–54

- Poinsot C, Baeyens B, Bradbury MH (1999) Experimental and modeling studies of caesium sorption on illite. *Geochim Cosmochim Acta* 63:3217–3227
- Qin H, Yokoyama Y, Fan Q, Iwatani H, Tanaka K, Sakaguchi A, Kanai Y, Zhu J, Onda Y, Takahashi Y (2012) Investigation of cesium adsorption on soil and sediment samples from Fukushima Prefecture by sequential extraction and EXAFS technique. *Geochem J* 46:297–302
- Redlich O, Peterson DL (1959) A useful adsorption isotherm. *J Phys Chem* 63:1024–1024
- Schnurr A, Marsac R, Rabung T, Lützenkirchen J, Geckeis H (2015) Sorption of Cm (III) and Eu (III) onto clay minerals under saline conditions: batch adsorption, laser-fluorescence spectroscopy and modeling. *Geochim Cosmochim Acta* 151:192–202
- Tamura K, Kogure T, Watanabe Y, Nagai C, Yamada H (2014) Uptake of cesium and strontium ions by artificially altered phlogopite. *Environ Sci Technol* 48:5808–5815
- Tan X, Fang M, Wang X (2010) Sorption speciation of lanthanides/actinides on minerals by TRLFS, EXAFS and DFT studies: a review. *Molecules* 15:8431–8468
- Tournassat C, Tinnacher RM, Grangeon S, Davis JA (2018) Modeling uranium (VI) adsorption onto montmorillonite under varying carbonate concentrations: a surface complexation model accounting for the spillover effect on surface potential. *Geochim Cosmochim Acta* 220:291–308
- Van Rompaey K, Van Ranst E, De Coninck F, Vindevoel N (2002) Dissolution characteristics of hectorite in inorganic acids. *Appl Clay Sci* 21:241–256
- Wang W, Shi L, Wu H, Ding Z, Liang J, Li P, Fan Q (2023) Interactions between micaceous minerals weathering and cesium adsorption. *Water Res* 238:119918
- Wu H, Qiang S, Fan Q, Zhao X, Liu P, Li P, Liang J, Wu W (2018) Exploring the relationship between Th (IV) adsorption and the structure alteration of phlogopite. *Appl Clay Sci* 152:295–302
- Wu L, Liao L, Lv G (2015) Influence of interlayer cations on organic intercalation of montmorillonite. *J Colloid Interface Sci* 454:1–7
- Yamamoto T (2012) Radioactivity of fission product and heavy nuclides deposited on soil in Fukushima Dai-Ichi Nuclear Power Plant accident: Fukushima NPP Accident Related. *J Nucl Sci Technol* 49:1116–1133
- Yu S, Wang X, Chen Z, Tan X, Wang H, Hu J, Alsaedi A, Alharbi NS, Guo W, Wang X (2016) Interaction mechanism of radionickel on Na-montmorillonite: influences of pH, electrolyte cations, humic acid and temperature. *Chem Eng J* 302:77–85
- Zachara JM, Smith SC, Liu X, McKinley JP, Serne RJ, Gassman PL (2002) Sorption of Cs+ to micaceous subsurface sediments from the Hanford site, USA. *Geochim Cosmochim Acta* 66:193–211
- Zhang C, Liu X, Lu X, He M, Meijer EJ, Wang R (2017) Surface complexation of heavy metal cations on clay edges: insights from first principles molecular dynamics simulation of Ni (II). *Geochim Cosmochim Acta* 203:54–68
- Zhang K, Li Z, Qi S, Chen W, Xie J, Wu H, Zhao H, Li D, Wang S (2022) Adsorption behavior of Cs (I) on natural soils: batch experiments and model-based quantification of different adsorption sites. *Chemosphere* 290:132636
- Zhang K, Chen W, Lu M, Li Z, Qi S, Fan Q, Zhao H, Yang J, Li D, Zhang J (2023) Adsorption forms of cesium in specific soils based on EXAFS spectroscopic investigations and sequential extraction experiments. *J Radioanal Nucl Chem* 332:527–538
- Zhang Y, Zhao H, Fan Q, Zheng X, Li P, Liu S, Wu W (2011) Sorption of U (VI) onto a decarbonated calcareous soil. *J Radioanal Nucl Chem* 288:395–404

**Publisher's Note** Springer Nature remains neutral with regard to jurisdictional claims in published maps and institutional affiliations.

Springer Nature or its licensor (e.g. a society or other partner) holds exclusive rights to this article under a publishing agreement with the author(s) or other rightsholder(s); author self-archiving of the accepted manuscript version of this article is solely governed by the terms of such publishing agreement and applicable law.